Beam Waveguide and Receiver Optics for the SMA

Scott Paine, D. Cosmo Papa, R. Louie Leombruno, Xiaolei Zhang, and Raymond Blundell

Harvard-Smithsonian Center for Astrophysics,
60 Garden Street, Cambridge, MA 02138, USA

Abstract

This paper gives an outline of the optics design for the Submillimeter Array. It emphasizes the natural frequency-independence and simplicity of Fresnel imaging principles as the starting point for the optics design, with multi-mode Gaussian beam methods used as a computational tool for working out the detailed behavior. A calculation of the coupling loss at the beam waveguide mirrors is presented as an example of the design method.

Introduction

The Submillimeter Array (SMA), currently under construction by the Smithsonian Astrophysical Observatory, will be a submillimeter interferometer initially comprising six 6-meter antennas configurable on baselines ranging from 9 meters to 465 meters. The completed array will ultimately be outfitted with up to eight receivers housed in a single cryostat for each antenna covering all atmospheric windows from 176 GHz to 900 GHz. This paper presents an overview of the SMA optics, with emphasis on the Fresnel imaging approach used for the optics design.

The body of the paper is divided into three sections. The first describes the physical layout of the receiver and beam waveguide optics. This is followed by a section on the principles of the optics design. The main point of this section is to illustrate the use of an approach to the design of broadband systems which takes Fresnel imaging as a starting point, as opposed to approaches which focus on the propagation of a particular Gaussian mode or mode set. From this viewpoint, multi-mode Gaussian beam methods
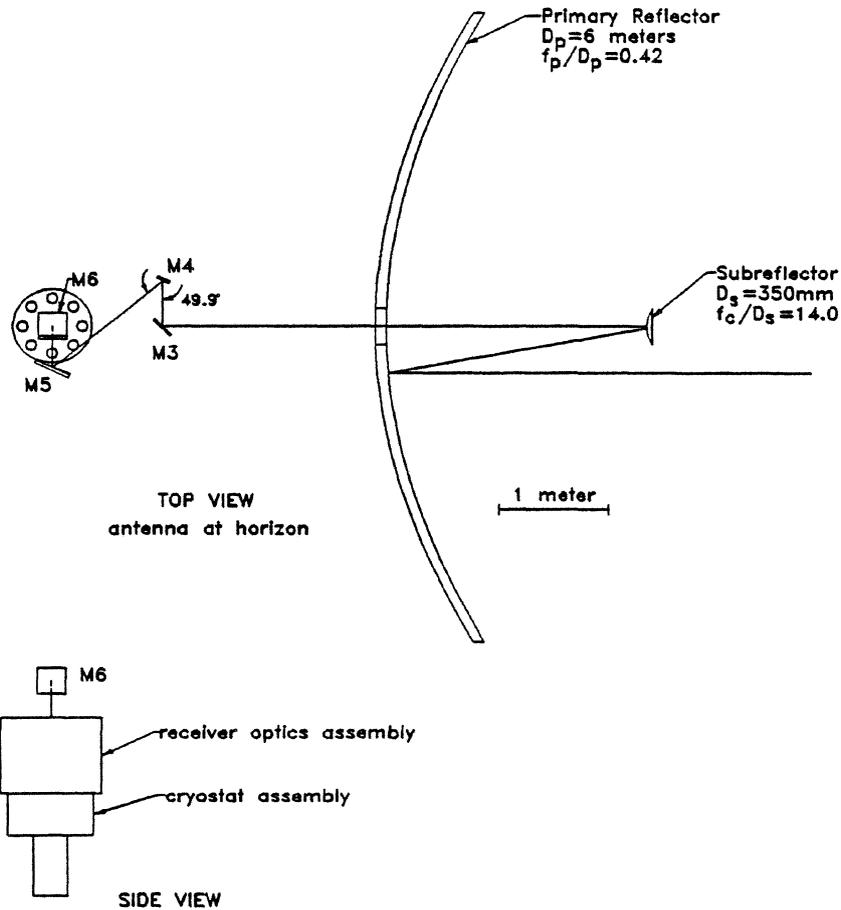
Figure 1 - SMA antenna optics layout

are a tool for handling propagation between image planes, with a particular mode set chosen to optimize computational efficiency for the design problem at hand. A final section will illustrate the application of this method to the detailed design of the optics, using a calculation of the coupling loss at one of the beam waveguide focusing mirrors as an example.

Optics Layout

The overall layout of the SMA antenna optics is illustrated schematically in Fig. 1. A 6-meter diameter paraboloidal primary reflector with focal ratio f/D=0.42 is combined with a 350 mm diameter hyperboloidal secondary with an effective focal ratio at the Cassegrain focus of 14.0. Mirrors M3 through M6 form a beam waveguide (Fig. 2) which
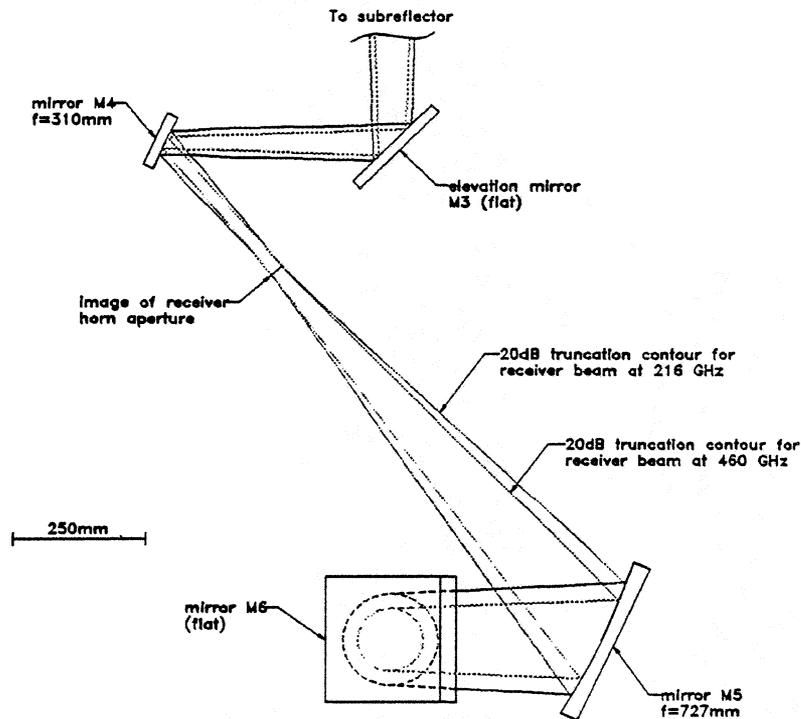
To subreflector

mirror M4
f=310mm

elevation mirror
M3 (flat)

Image of receiver
horn aperture

20dB truncation contour for
receiver beam at 216 GHz

20dB truncation contour for
receiver beam at 460 GHz

|___250mm___|

mirror M6
(flat)

mirror M5
f=727mm

Figure 2 - Beam waveguide mirrors

directs the beam from the antenna vertically downward into the receiver optics assembly. The folded Naysmith configuration of the beam waveguide was adopted for two primary reasons. First, it allows the receivers to operate in a fixed orientation relative to gravity, avoiding mechanical disturbance of the receivers when the antenna is moved. Second, it fits within the compact receiver cabin design required for the SMA antennas.

A schematic showing the receiver optics layout and the arrangement of receivers in the cryostat is shown in Fig. 3. The beam from mirror M6 is split into two orthogonally polarized beams by a diplexer consisting of a polarizing wire grid and mirror which rotate independently about the axis of the incoming beam. The two orthogonally polarized beams are directed by the diplexer to a pair of receivers oriented 90° apart in the cryostat assembly. The eight receiver positions in the cryostat are divided into two groups: four low-frequency ($\nu < 360$ GHz) positions and four high-frequency ($\nu > 330$ GHz) positions, arranged so that every right angle pair of receivers consists of one receiver from each
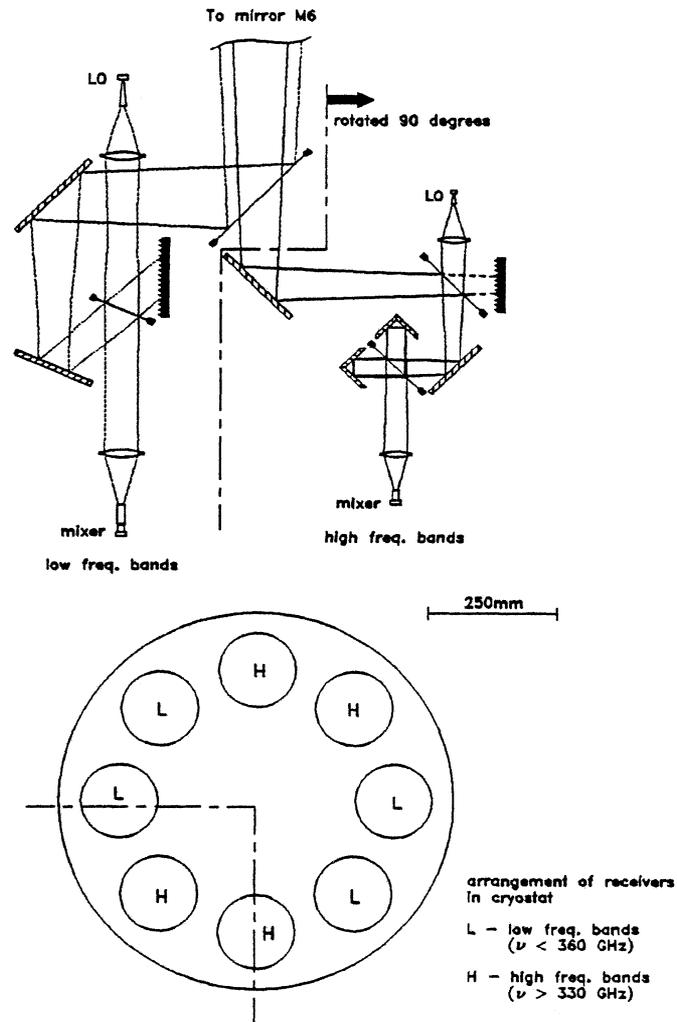
Figure 3 - Receiver optics layout. 20 dB truncation contours for the receiver beam are shown at 216 GHz for the low-frequency optics and at 460 GHz for the high-frequency optics.

group. An overlapping pair of high- and low-frequency receiver bands will permit dual-polarization operation from 330 GHz to 360 GHz.

Because a large number of receivers will eventually be installed in the SMA, the receiver optics design has been kept as simple as possible. For example, apart from the horn-lens combinations, which are unique to each receiver band, the optics for all four receivers in each group are identical. No focusing mirrors are used between the feed lens and the central diplexer, which simplifies the optical alignment of each individual receiver as well as the mutual co-alignment of all the receiver beams. The local-oscillator (LO)

injection scheme for the low-frequency receivers is a simple rotatable wire-grid polarizer adjusted to transmit a small fraction of the LO power and reflect nearly all of the signal power, with the reflected LO power diverted to an absorbing load. It is anticipated that sufficient LO power will be available at these frequencies to limit the signal loss using this scheme to 1% or less. Since available LO power for the high-frequency bands will be more limited, the LO for these bands will be coupled to the mixer via a Martin-Puplett diplexer. No sideband filtering is planned for the receiver optics at present. This results in a considerable simplification of the optics at the expense of somewhat increased system temperature for single-sideband operation. When the array is operating as an interferometer, phase switching techniques will be used to separate the upper and lower sidebands.

The mixer block, feed horn, and lens for each receiver are mounted in the cryostat on a removable cylindrical insert. It is anticipated that scalar feeds will be used for frequency bands up to at least 720 GHz. So far, prototype scalar horns have been produced for the SMA up to 520 GHz, using the design described in reference [1]. The lenses have been designed using the procedure described by Lee in Ref. [2] to provide a quadratic phase transformation free from amplitude distortion. The horn-lens combinations are designed to produce a virtual image of the horn aperture located behind the horn which is standardized for all receiver inserts, as will be described in the next section.

Optics Design

Traditionally, quasioptical feed systems for reflector antennas have been designed using fundamental-mode Gaussian beam analysis [3]. More recently, the importance of including higher-order modes in the analysis has been demonstrated [4],[5]. Nevertheless, the emphasis has been on propagation of a particular mode set and its associated phase slippage through the entire optical system. We have adopted a somewhat different approach which emphasizes the simplicity and natural frequency-independence of Fresnel imaging relations as a starting point for design. Multi-mode Gaussian beam techniques are
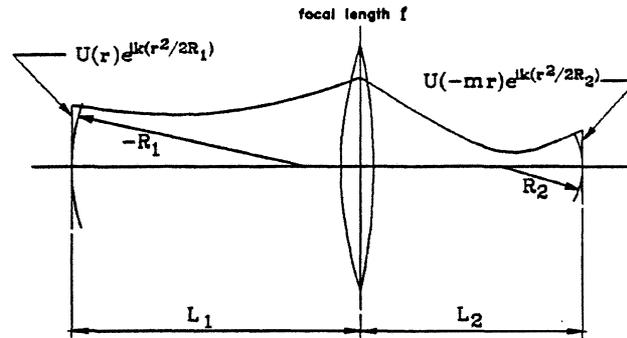
Figure 4 - Fresnel imaging by a focusing element.

then used as a computational tool for working out the propagation of the beam between images, with the choice of an appropriate mode set for a given calculation motivated chiefly by consideration of minimum computational effort to achieve the desired numerical accuracy [6]. The use of Fresnel imaging principles in beam waveguide design is not new. Previous work has discussed Fresnel imaging in the context of single-mode [7] and multi-mode [5] beam waveguide design. Here, our purpose is to stress the usefulness of a global application of imaging principles to broadband system design.

The basic Fresnel imaging relations for a single focusing element are illustrated in Fig. 4. For the parameters shown in the figure, the following relations hold for the fields at the images on either side of the focusing element:

$$\frac{1}{L_1} + \frac{1}{L_2} = \frac{1}{f}$$

Eq. 1

$$\frac{1}{R_2} = \frac{1}{L_2} \cdot \left[1 + \frac{L_1}{L_2} \cdot \left(1 + \frac{L_1}{R_1} \right) \right]$$

Eq. 2

$$m = \frac{L_1}{L_2}$$

Eq. 3

Eqs. 1-3 are derived using Gaussian beam propagation formulas in Ref. [7]; a more general derivation is given in Ref. [8]. The wavefront radii R_1 and R_2 at the two image planes represent quadratic phase curvatures which, when factored out of the fields in their respective image planes, yield two fields which are simply scaled and inverted images of one another. Note that this imaging property is independent of frequency.

The Fresnel imaging equations form the basis for the design of a broadband imaging beam waveguide which functions to image a plane at the receiver feed where the form and phase curvature of the field is independent (or nearly-independent) of frequency onto the subreflector. The phase curvature radius of the image at the subreflector is set equal to the Cassegrain focal length. The size of the image at the subreflector depends on the application— for a radio interferometer the goal is to maximize the antenna gain; in other applications considerations such as reduced sidelobes may be important. The choice of the image plane at the receiver depends on the nature of the feed. For horns, the form and phase curvature of the aperture field can be made nearly independent of frequency over a broad bandwidth. For other types of feeds such as quasioptical antennas, the choice of the optimum frequency-independent image plane has not been investigated thoroughly.

The design of the SMA optics presents a typical case for application of Fresnel imaging principles. The main constraints on the design were the size of the secondary mirror, the permissible range of locations for the beam waveguide mirrors within the allotted receiver cabin space, and the optical path length through the rotating diplexer and the receiver optics. The desire to avoid focusing mirrors in the individual receiver optics led to a requirement that all of the feed-lens combinations for the various receivers present the same image to the beam waveguide in order that any pair of receivers could simultaneously illuminate the antenna. A maximum size of 75 mm for the windows in the cryostat was established based on considerations of heat load and overall space available.

As a starting point for establishing the common image plane for all of the feed-lens combinations, the beam at the lowest frequency was assumed to have flat phase at the cryostat window in order to minimize the size of the low-frequency receiver optics and of mirrors M5 and M6. Since it was both undesirable and unnecessary for the lenses and windows at higher frequencies to be as large, the image plane was chosen to be located behind the feeds with negative phase curvature, producing a "virtual feed" located behind the real feeds as shown in Fig. 5. Choosing this location for the virtual feed allows the lenses to be smaller and hence thinner with increasing frequency, easing the problem of increasing absorption loss in the lens materials as well as reducing the heat load on the
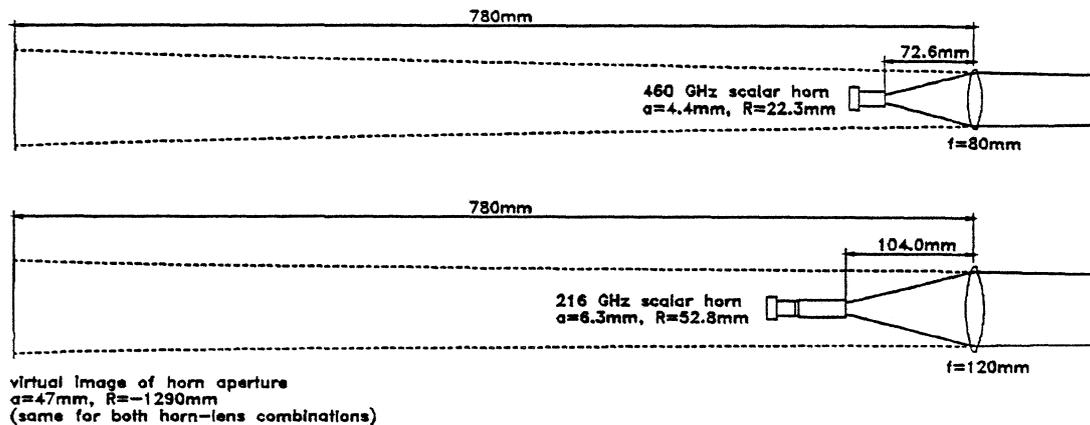
Figure 5 - Scalar horn-lens combinations for two receiver bands covering 176-256 GHz and 400-520 GHz. Both produce identical "virtual feeds" located behind the lens.

cryostat. Once the location of the virtual feed was established, the receiver optics were sized to reduce truncation effects to an acceptable level at the lowest frequency used in each receiver group (176 GHz for low-frequency receivers, 330 GHz for high-frequency receivers.) The truncation calculations were performed using multi-mode Gaussian beam methods described by Murphy et al. [9]. Lens diameters were chosen to minimize the product of truncation loss at the lens aperture and absorption loss through the center of the lens.

The virtual feed is imaged onto the subreflector by the beam waveguide consisting of mirrors M3 through M6. For scalar horns, an image of the truncated Bessel field at the feed aperture with 10.0 dB edge taper maximizes the antenna gain. The mechanical layout of the SMA antenna prevented the imaging from being accomplished with a single focusing mirror so two mirrors, M4 and M5, are used. For these mirrors, two design options were possible— two ellipsoidal mirrors, with an additional real image produced between M4 and M5, or an ellipsoidal M5 and hyperboloidal M4, with a virtual image behind M4. While the latter option would have resulted in a design with slower beams and hence more attractive from the standpoint of minimizing coupling loss and cross-polarization, the former option was chosen since the real image is a particularly good location for the receiver calibration loads and for the quarter-wave plate which will be used for circular polarization measurements near 345 GHz. Motivated by coupling loss

calculations of the kind described in the next section, the Z-shaped configuration shown in Fig. 2 for the beam waveguide mirrors was adopted to reduce the incidence angle, and hence the coupling loss, at the beam waveguide mirrors to an acceptable level.

Beam Waveguide Mirror Loss

Several mechanisms lead to beam coupling loss at focusing mirrors employed in beam waveguides [10]-[13]. For mirrors intended to couple two axially-symmetric beams, the change in beam divergence on either side of the mirror produces a geometric mismatch of the two beams across the mirror surface, with resulting coupling loss. For broadband mirrors, phase errors result in additional loss when the mirror is operated away from its design frequency. Finally, at points on the mirror away from the plane of incidence, the electric field of the incoming beam undergoes a rotation about the axis of propagation which produces a cross-polarization loss. With two similar mirrors located near images of one another, these losses can be minimized by using one mirror to partially cancel the effects of the other. For the SMA beam waveguide, this option was not feasible. Instead, the mirror losses have been held to a minimum by keeping the incidence angles small at M4 and M5 as mentioned above.

Mirror M5, which operates at a smaller effective focal ratio than M4 at all frequencies, contributes the greatest coupling loss— approximately four times that at M4. To estimate the coupling loss at M5, a method based on evaluating the aperture efficiency coupling integral across the mirror surface is used. Neglecting blockage and the smaller beam distortion caused by M4, a distant point source illuminating the antenna produces a uniform top-hat field distribution at the image of the subreflector between M4 and M5. This image is taken as the source plane for the beam on the sky side of M5. The source plane for the beam on the receiver side is the virtual feed, where the field is taken to be the truncated Bessel distribution produced by a scalar feed. (For the highest frequency bands, a different type of feed may actually be used.) The coupling between these two beams is then evaluated by direct numerical integration over the mirror surface. Based on the local conservation of the area-intensity product at the mirror surface [14], the coupling integral may be written as

$$C = \int_M (d\vec{a} \cdot \vec{S}_1)^{1/2} (d\vec{a} \cdot \vec{S}_2)^{1/2} E_1 E_2^* ,$$ **Eq. 4**

where E_1 and E_2 are the incident and reflected fields, normalized to unit power in each beam, and

$$\vec{S}_1 = \frac{\nabla\left[\arg(E_1)\right]}{\left|\nabla\left[\arg(E_1)\right]\right|}$$ **Eq. 5**

$$\vec{S}_2 = \frac{\nabla\left[\arg(E_2)\right]}{\left|\nabla\left[\arg(E_2)\right]\right|}$$ **Eq. 6**

are the local normals to the incident and reflected wavefronts.

Fig. 6 shows the power coupling CC^* evaluated from Eq. 4 over the range of SMA operating frequencies and for four different ellipsoids with the same effective focal length, but designed to match the on-axis wavefront curvatures of the beams on either side of the mirror at four different frequencies. The theoretical aperture efficiency in the absence of mirror distortion is 86.9%. Bearing in mind the approximation introduced by ignoring the effects of M4, the difference between this figure and the calculated coupling integral gives a measure of the loss at M5. The overall trend exhibited by all of the curves in Fig. 6 is primarily due to the geometric loss, which increases as the effective focal ratios at the mirror decrease towards low frequencies. The differences between the curves indicate the effects of phase loss due to operation away from the design frequency. For the SMA, a design frequency of 345 GHz has been chosen as a suitable compromise between the low-frequency loss (~3.8%) and the high-frequency loss (~1.8%). It is worth noting that the loss estimated this way is considerably higher than what would be expected based on the method in Ref. [11], which considers the loss for a fundamental-mode Gaussian beam. This point should be borne in mind when attempting to design high-efficiency feed systems. Increasing the angle of incidence at M5 from its present value of 25° up to 45° nearly doubles the loss at all frequencies, which was the reason for adding the additional flat mirror M6 to effect the 90° turn in the optical path.

In performing the above calculation, two different Gauss-Laguerre mode sets are used to represent the beams on either side of the mirror. To achieve convergence of the
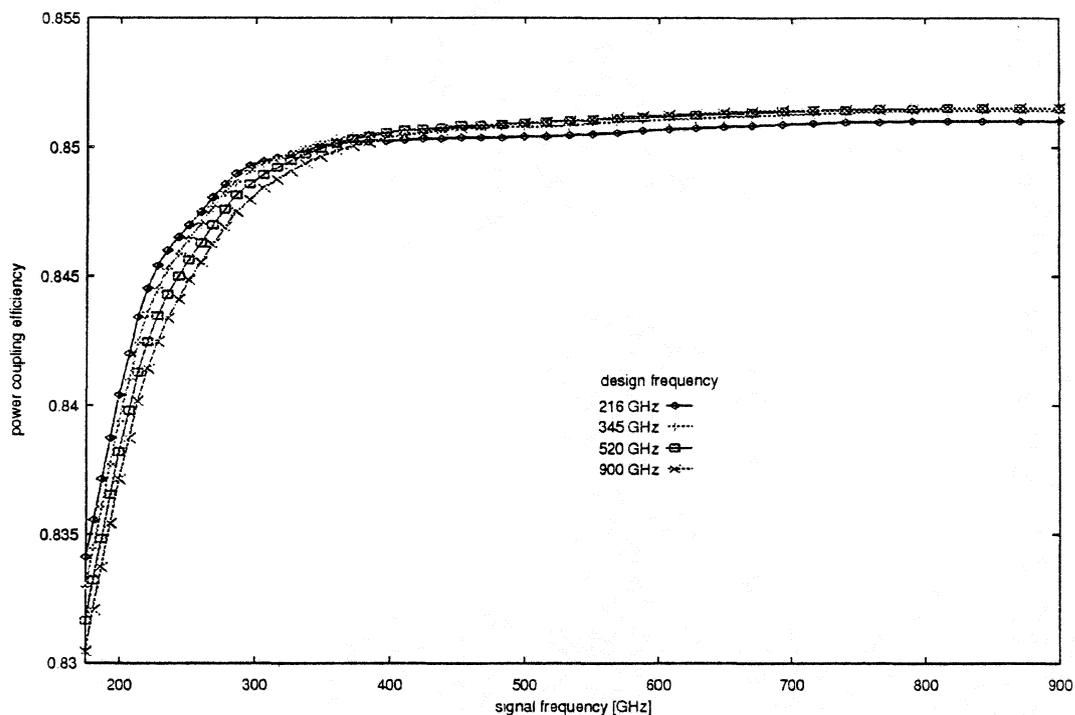
Figure 6 - Aperture efficiency coupling integral evaluated at the surface of mirror M5. In the absence of the mirror loss mechanisms discussed in the text, the theoretical efficiency would be 0.869.

integral to a few parts in 10^4, a set of 10 modes with beam radius $w = 0.28 \cdot a_f$, where a_f is the radius of the horn aperture image, is used for the beam on the receiver side of the mirror, and a set of 20 modes with beam radius $w = 0.22 \cdot a_s$, where a_s is the radius of the subreflector image, is used for the beam on the sky side. The expansion coefficients for the scalar feed beam are calculated by numerical integration; those for the uniform top-hat are calculated using the recursion formulas given in Ref. [9]. To calculate the field at a point on the mirror surface, these two beams are each propagated to the surface point from their respective source planes using the usual multi-mode beam propagation methods.

Conclusions

This paper has presented an outline of the optics for the Submillimeter Array telescopes as an example of a Fresnel imaging approach to broadband millimeter- and submillimeter-

wave optical system design. Using the calculation of the beam waveguide mirror coupling loss as an example, it has shown how this point of view leads naturally to the identification of appropriate source planes and mode sets for calculations related to the detailed analysis of system performance.

References

[1] X. Zhang, "Design of Conical Corrugated Feed Horns for Wide-Band High-Frequency Applications," *IEEE Trans. Microwave Theory Tech.,* MTT-41 1263 (August 1993.)

[2] J. J. Lee, "Dielectric Lens Shaping and Coma-Correction Zoning, Part I: Analysis," *IEEE Trans. Antennas Propagat.,* AP-31 211 (January 1983.)

[3] P. Goldsmith, "Quasi-Optical Techniques at Millimeter and Submillimeter Wavelengths," Chapter 5 in Infrared and Millimeter Waves, Vol. 6, K. Button, ed. Academic Press (1982.)

[4] J. W. Lamb, "Quasioptical Coupling of Gaussian Beam Systems to Large Cassegrain Antennas," *International Journal of Infrared and Millimeter Waves* 7 1511 (July 1986.)

[5] R. Padman, J. A. Murphy, and R. E. Hills, "Gaussian Mode Analysis of Cassegrain Antenna Efficiency," *IEEE Trans. Antennas Propagat.* AP-35 1093 (October 1987.)

[6] See J. W. Lamb, "Beam-mode expansion applied to focal-region fields," *IEE Proceedings-H* 139 513 (December 1992) for an example of basis optimization as well as a demonstration of the relationship between Gaussian beam-modes and Fourier optics.

[7] Ta-Shing Chu, "An Imaging Beam Waveguide Feed, "*IEEE Trans. Antennas Propagat..* AP-31 614 (July 1983.)

[8] J. W. Goodman, Introduction to Fourier Optics, McGraw-Hill (1968.)

[9] J. A. Murphy, Aidan Egan, and S. Withington, "Truncation in Millimeter and Submillimeter-Wave Optical Systems," *IEEE Trans. Antennas Propagat.* AP-41 1408 (October 1993.) Also see J. A. Murphy, S. Withington, and A. Egan, "Mode Conversion at Diffracting Apertures in Millimeter and Submillimeter Wave Optical Systems," *IEEE Trans. Microwave Theory Tech..* MTT-41 1700 (October 1993.)

[10]   M. J. Gans, "Cross-Polarization in Reflector-Type Beam Waveguides and Antennas," *Bell System Technical Journal* 55 289 (March 1976.)

[11]   J. A. Murphy, "Distortion of a Simple Gaussian Beam on Reflection from Off-Axis Ellipsoidal Mirrors," *International Journal of Infrared and Millimeter Waves* 8 1165 (September 1987.)

[12]   J. C. G. Lesurf, Millimetre-wave Optics, Devices, and Systems, Adam Hilger (1990.)

[13]   S. Withington and J. A. Murphy, "Gaussian-mode Analysis of 'Thin' Mirrors," *Fourth Int. Symp. on Space Terahertz Technology* pp.211-222 (1993.)

[14]   M. Born and E. Wolf, Principles of Optics, 6th ed. Pergamon (1980) (section 3.1.2)